Optimization of the magnetocaloric effect in arrays of Ni_3Pt nanomagnets

S. Vorobiov[a, b], D. Tomasova[a], V.Girman[a], H. You[c], E. Čižmár[a], M. Orendáč[a], V. Komanicky [a,*]

[a]P.J. Šafárik University, Park Angelinum 9, 04013 Košice, Slovakia
[b]Sumy State University, Rymskyi-Korsakov Str. 2, Sumy 40007, Ukraine
[c]Argonne National Laboratory, Argonne, Illinois 60439, United States

*Corresponding author: e-mail: vladimir.komanicky@upjs.sk

Abstract

Structural parameters of nanomagnet arrays have been systematically adjusted in order to study and to maximize the magnetocaloric effect. Optimum technological parameters were experimentally established and arrays of nanomagnets based on Ni_3Pt nanoparticles with a different structure period (1, 2, 3 μm) and two different heights (1.2 and 1.9 μm) were fabricated using electron-beam lithography followed by electrodeposition. The obtained arrays have a phase composition of fcc-Ni_3Pt, which remains unchanged after annealing. It was shown that a change in the period of the nanomagnet arrays leads to a change in the magnitude of the magnetocaloric effect and the operating temperature range. Also, changes in the height of nanomagnets from 1.2 to 1.9 μm lead to an increase in the magnetocaloric response by more than 30%.

Keywords
Arrays of nanomagnets; Electron-beam lithography; Electrochemical deposition; Magnetocaloric effect.

1. Introductions

In recent years, there has been a rapid miniaturization of electronic components to nanoscopic scale. Such a trend requires the development of new methods and technological procedures that will ensure the operation of devices while reducing their size. One of the important tasks which need to be solved to ensure the reliable operation of nanoscale devices is maintaining the right operating temperature. The traditional vapor compression refrigeration is extremely inefficient for cooling nanostructured devices.

Magnetic refrigeration (MR) using nanoscale devices or materials constitute a promising choice to fulfill this requirement [1-4]. The working principle of magnetic refrigeration is based on the magnetocaloric effect (MCE). Compared with conventional refrigeration, MR is more energy efficient and environmentally friendly [1-4]. The difference between conventional refrigeration that uses harmful refrigerants is that MRs generally uses harmless liquid for cooling and solid magnetic materials as the refrigerants.

The most challenging task is to search for new materials with their MCE sufficiently large for the MR applications [1-5]. The highest value of MCE is observed in rare - earth based materials but their commercial use is limited due to their high cost and limited supply. Hence, research has focused on finding rare earth free magnetic and magnetocaloric materials. Heusler alloys [6-8], high entropy alloys [9-10] and magnetic nanoparticles [11-12], are promising alternatives to traditional magnetocaloric materials. This is primarily due to the possibility of relatively easy manipulation of the geometric distribution of magnetic nanoparticles by traditional deposition methods [11].

Changing geometry of magnetic nanoparticles systems, such as the size and the distance between the particles (both freestanding and placed in a nonmagnetic matrix) allows to tune magnetic properties of the system, that is useful for obtaining a desired MCE response [13-14].

The key point of searching for the most suitable materials for practical usage in MR is not only the type of material but also the finding of suitable geometric arrangements and the conditions for their implementation, which would give the opportunity to maximize MCE [15-17]. For instance, theoretical modeling of systems based on one-dimensional (1D) structures formed as chains of single-domain particles, where the length of the chain would be much larger than the diameter [17] shows that such a system will exhibit high magnetic anisotropy.

The approach considered in this work was based on the fabrication of nanomagnet arrays by electron beam lithography with a precisely controlled size and the distance between magnets in a wide range. This would allow us to study collective as well as individual nanomagnet contributions to the magnetic behavior of these systems. Ni_3Pt composition was selected as a compromise between high magnetic moment and ordering temperature below 400 K [18]. These systems can be prepared by relatively simple electrodeposition method from aqueous solutions [19] with good control of the composition and size of particles. To our knowledge, this is the first study of such type of nanomagnet arrays based on Ni-Pt alloy and our main goal was to tune systematically their magnetic properties by geometric arrangement of nanomagnets with the aim to maximize MCE and shift the application region close to the room temperature.

2. Results and discussion

2.1 Fabrication of nanomagnet arrays

The fabrication of arrays of nanomagnets based on Ni_3Pt was carried out using electron-beam lithography and electrochemical deposition method. At the first stage, electron-beam lithography was used to form masks in a resist for further electrochemical deposition. For this, a high-resolution positive resist for direct write e-beam polymethyl methacrylate (NANO 950 PMMA A, MicroChem) was spin-coated on glassy carbon substrates (HTW, Germany) with the size of 0.5 × 0.5 mm. To improve the electrical conductivity of the substrate a thin Au film with a thickness of 10 nm was sputtered by magnetron deposition (ATC-Orion 8 Sputtering Systems) on the substrate surface. The desired thickness of resist was achieved by the spin speed selection (optimum speed in our case was 4000 rpm) and the time (optimal value 50 sec). To obtain several microns thick resist layers the resist density was also increased by reducing the concentration of solvent (Anisole). After spin-coating, the resist layer was prebaked at 170°C during for 30 sec.

Electron microscope Tescan, model VEGA, was used for electron-beam lithography scanning. The desired lattice period between elements in a square lattice of the structures was 1, 2, and 3 microns. The size of masks in resist layer was 2×2 mm. One of the main tasks during the mask forming was to provide the same size of the elements of the structure (nanopore) with changing their periodicity. To establish the optimal parameters of the obtained masks a series of dose test experiments were conducted. The beam current (0.7 – 1.1 nA), exposure time (0.01 – 0.5 ms) and standard dose (200 – 550 $\mu C/cm^2$) was tweaked to obtain desired results. After exposure by an electron beam, the sample was placed in a solution of 4-Methyl-2-pentanone (MIBK) and isopropyl alcohol (IPA) (1:3 MIBK : IPA).

The obtained masks in resists were characterized by atomic force microscopy (Bruker, model ICON) in tapping mode. Pore diameter dependencies on exposure time at the different distance between the pores and various resist thicknesses are shown in Figure 1(a). Figure 1(b) shows the typical dependencies of the nanopores size depending on the exposure time for resist thickness of 2 μm at a dose of 250 μC/cm^2.

To minimize distortions in the fabrication of mask due to write field limitations the whole array with area 2 × 2 mm^2 was composed from square fragments with size 0.2 × 0.2 mm^2. This approach allowed to form the matrix of the required size with high accuracy.

The formation of arrays of Ni_3Pt nanomagnets in the resist mask was carried out using electrochemical deposition. The three electrode configuration was used: the sample as the working electrode, Pt counter electrode. The applied potential (-0.6 V) is given with respect to that of the reference electrode (saturated calomel electrode-SCE, silver chloride electrode Ag/AgCl). Electrolyte for electrodeposition contained 0.003 mol/l K_2PtCl_4 + 0.1 mol/l $NiCl_2$ + 0.5 mol/l NaCl (pH = 2.5) [19]. The electrodeposition time, for selected pore size (500 nm) and two different pore depths (1.2 μm and 1.9 μm) ranged from 200 to 500 seconds. After electrochemical deposition, the samples were placed into acetone for 15 minutes to remove the resist. The whole cycle of the technological process is shown in Figure 2. Once the structures have been formed, the arrays were characterized by scanning electron microscopy. Estimated number of defects in the obtained arrays that may occur due to substrate imperfections and limitations in electrochemical deposition does not exceed 0.2%.

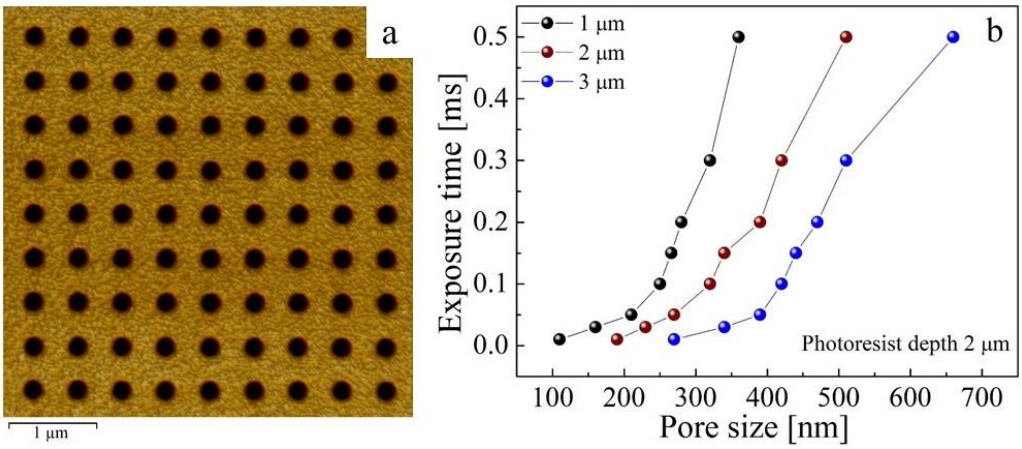

Fig. 1. (a) AFM image of the fragment of the fabricated mask in the resist. (b) Dependence of pore diameter on the parameters of the electron beam fabrication process.

We also determined the concentration of components after electrochemical deposition and their distribution in the volume of individual elements of nanostructures by Energy Dispersive X-Ray Spectroscopy (EDS) analysis. The results show that regardless of the period and the diameter and height of the obtained structures the deviation from the specified concentration does not exceed 2 % for all samples. In Figure 3 the elemental map from an array of nanostructures based on Ni_3Pt is shown. As seen from this figure, the elements are evenly distributed throughout the volume of the structure fragment. This analysis is performed for each received structure before carrying out research of magnetic characteristics. Maximum permissible deviation of the final concentration was not more than 2 at. %

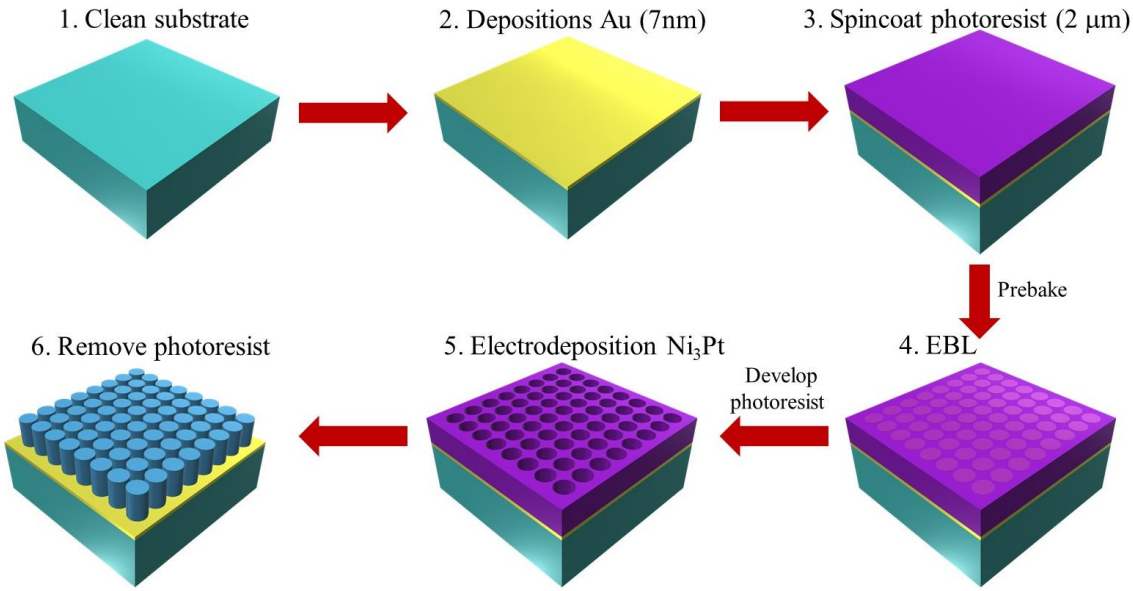

Fig. 2. Scheme of the technological process of obtaining arrays of nanomagnets

The shape of the nanopores in the resist is dependent on the scattering profile of the primary electron beam in the resist and also an avalanche of secondary electrons. Therefore we carefully optimized the thickness of the resist and also the energy of the primary electron beam in order to obtain a cylindrical profile of the nanopore. Figure 4 shows the image of a fragment of an array of nanostructures with different periodicity (1 (a), 2 (b) and 3 (c) microns) from the top (a-c) and at an angle of 70°(d). It can be seen the obtained nanomagnets have a cylindrical shape.

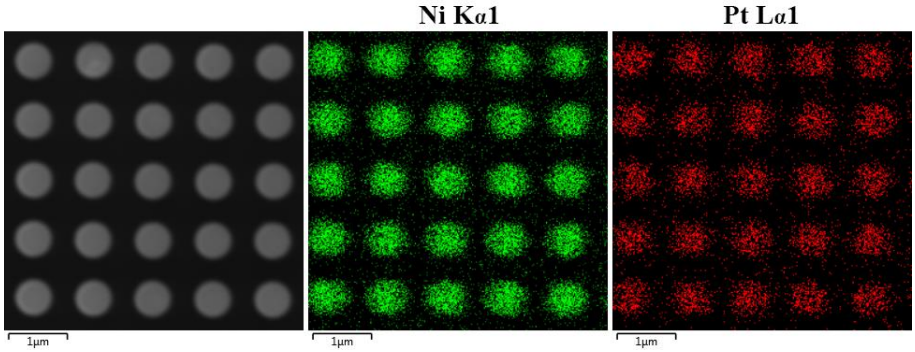

Fig. 3. SEM and EDS elemental mapping of the fragment of the received matrix

The phase composition of nanomagnet arrays after the electrochemical deposition was investigated using an X-ray diffractometer Rigaku Ultima IV (using K_α radiation of the cobalt anode). The average crystallite size L is determined by the Scherrer equation.

The crystal structure of the samples was also studied by a high-resolution transmission electron microscope (JEOL-TEM 2100F 200 kV). To improve the crystallinity of nanomagnets and to reduce defects in the crystal structure, the annealing of these systems in the atmosphere of N_2 was performed for 1 hour at a temperature of 800 K. After annealing, we again performed structural analysis by X-ray diffraction and EDS analysis.

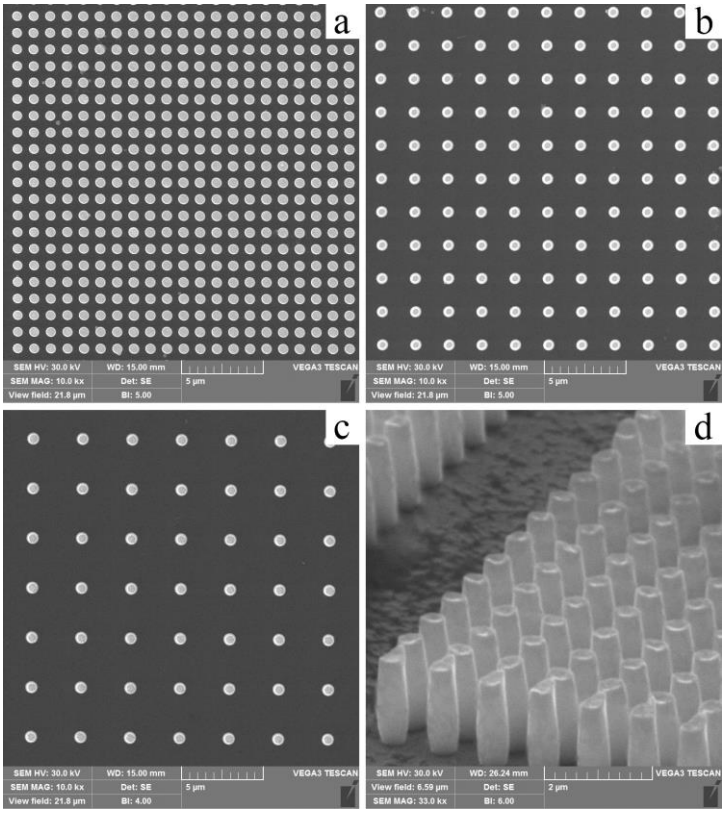

Fig. 4. SEM image of a fragment of an array of nanomagnets based on Ni_3Pt

2.2 Structural characterization

Figure 5(a) shows the X-ray diffraction patterns obtained from arrays of nanomagnets with a structure period 1 μm after electrochemical deposition and after thermal annealing up to 800 K. It should be noted that the annealing temperature was chosen based on the phase diagram of the binary Ni-Pt system [20]. Up to 800 K no phase transitions occur. Studies of the phase composition after electrochemical deposition have shown that the obtained samples have a phase composition of fcc-Ni_3Pt with a crystal lattice parameter $a_{aver.} = 0{,}362$ nm and an average crystallite size of $d_{aver.} = 8$ nm. There is no phase separation because there are no peaks which would correspond to fcc-Ni and fcc-Pt, shown by dashed lines in Figure 5(a)). Data on the average crystallite size is also confirmed by data obtained from the TEM image. A typical image of the crystal structure is shown in Figure 5(b). It can be seen that nanomagnet cylinders are polycrystalline with average grain size 6-8 nm.

After annealing up to 800 K the intensity of Ni_3P peak to is increasing, with a decrease in full width half maximum (Figure 5(a)). This indicates the improvement of the crystallinity of the nanomagnet arrays. The average crystallite size increases to the value of $d_{aver.} = 27$ nm , which is additionally confirmed by the data obtained from the TEM image (Figure 5(c)). The phase composition remains unchanged and the presence of the fcc-Au peak near the fcc-Ni_3Pt peaks is explained by crystallization processes in the gold layer, which was used to improve the conductivity of the substrate during electrochemical deposition. The parameter of the crystal lattice is $a_{aver.} = 0{,}366$ nm, which indicates a decrease in the number of point defects.

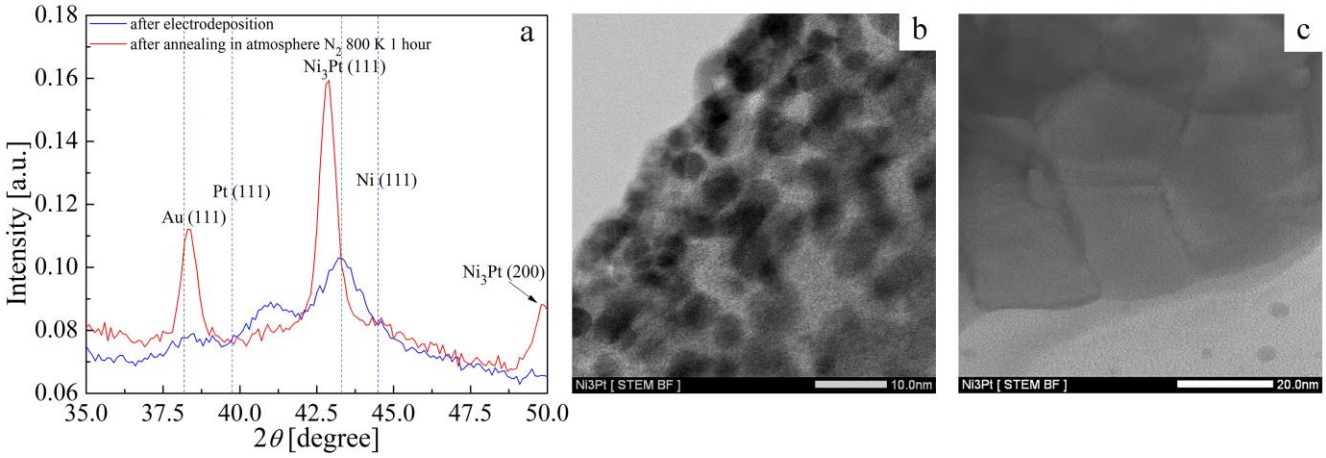

Fig. 5. (a) X-ray diffraction patterns of Ni_3Pt before (blue) and after (red) annealing in N_2 atmosphere at 800 K. (b) TEM image of the crystalline structure of Ni_3Pt nanomagnets before (b) and after (c) annealing.

2.3 Magnetic properties

The investigation of the magnetic properties of the bulk Ni_3Pt sample represented the initial point in the study of the magnetothermal characteristics of the arrays of nanomagnets. The bulk sample was produced by arc melting in Ar atmosphere. The final composition of the components was monitored by EDS analysis, which showed a deviation of the concentration over the entire volume of not more than 0.5 at.%. The bulk sample acted as a reference sample, which enabled to estimate in more detail the effect of the structure period on the magnetic characteristics of arrays of nanomagnets.

Thermomagnetic measurements of the bulk sample of Ni_3Pt M(T) in the zero-field-cooled (ZFC) and field-cooled (FC) mode were performed using a commercial SQUID magnetometer (Quantum Design MPMS3) carried out in the temperature range 2 – 400 K with applied magnetic field of 2 mT. The sample was first measured in the ZFC mode, i.e., the sample was cooled to the lowest measured temperature in zero magnetic field, then the field was switched on and the measurement was made while warming up the sample to temperature 400 K. Then the magnetic field was kept on, the sample was cooled (FC mode) and the measurement was made again while warming up. In order to evaluate magnetocaloric behavior, the measurement of the isothermal magnetization curves was conducted up to 2 T in the temperature range from 200 K to 400 K.

The isothermal magnetic entropy change ΔS_M has been calculated using the Maxwell relation [21]:

$$\Delta S_M = (T, \Delta B) = \int_{B_i}^{B_f} \frac{\partial M(T, B)}{\partial T} dB,$$

where B_i and B_f represent the initial and final magnetic fields, respectively.

The temperature dependence of the magnetization of the bulk sample of Ni_3Pt results of these measurements are presented in Figure 6(a). The bifurcation of ZFC and FC magnetization curves observed at 360 K indicates long-range ordering in Ni_3Pt in accordance with previous reports [18]. In addition, the temperature dependence of the change in entropy from a bulk sample of Ni_3Pt under isothermal magnetization from 0 T to different values of the final field from 0.5 T to 2 T is shown in Figure 6(b). As anticipated, the magnetocaloric response is focused in the critical region and the position of its maximum is very little affected by the magnitude of the final magnetic field.

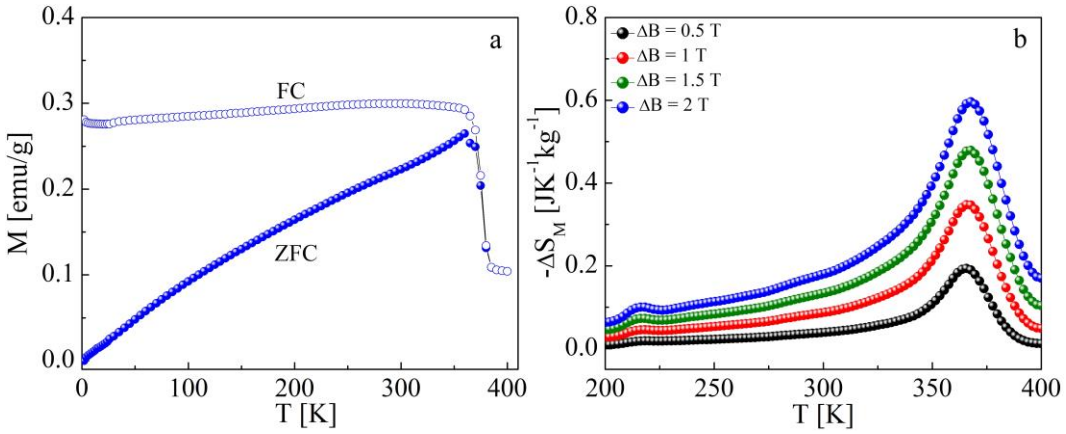

Fig. 6. (a) ZFC and FC magnetization curves obtained from bulk Ni_3Pt at in a measuring field and cooling field of 2 mT. (b) Temperature dependence of the isothermal entropy change in bulk Ni_3Pt at different magnetic field change.

Having the bulk reference data, the temperature dependence of ZFC and FC magnetization in the measuring (and cooling) field of 10 mT was performed in two geometries, with the field applied parallel and perpendicular to the array substrate (parallel and perpendicular orientation). As can be seen from Figure 7, the increase in the period of the structure leads to a shift of the blocking temperature into the region of lower temperatures. Notably, the lowest blocking temperature was found for the array with the structure period of 2 μm.

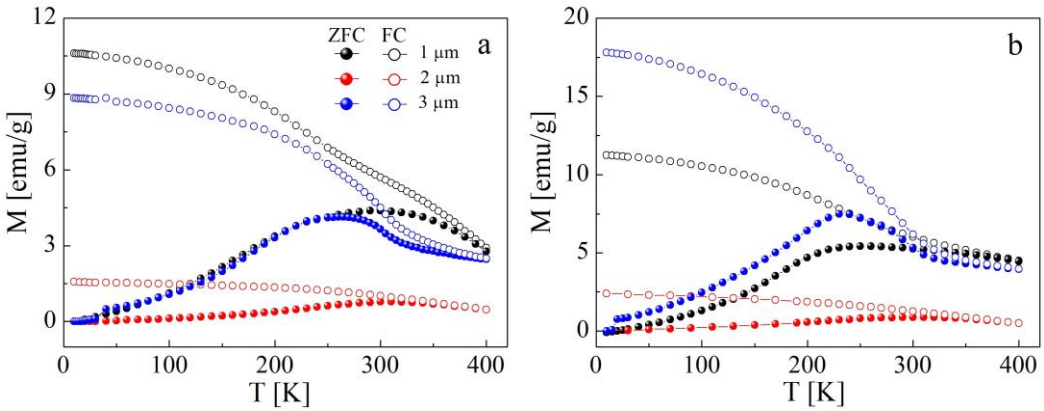

Fig. 7. ZFC-FC curves obtained from nanomagnet arrays based on Ni_3Pt at in a measuring field and cooling field of 10 mT: a) parallel orientation; b) perpendicular orientation.

Figure 8 shows the field dependence of the magnetization studied at 300 K (after warming the sample up to 400 K and cooling back in zero magnetic field) for arrays of nanomagnets with a different periodicity of the structure for both magnetic field orientations. Regardless of the measurement geometry, the maximum value of *M*(B) is observed at the value of the period of the structure of the nanomagnet array of 1 μm. As the distance between the nanomagnets increases, the magnetization from the applied external magnetic field decreases. Obviously, the concentration of nanomagnets in the array plays a role, however, nonmonotonic behavior was observed. More specifically, the smallest value of *M*(B) is observed for the period of the structure of the nanomagnet array of 2 μm. Up to now, this fact has not been explained in detail and will be a subject of future investigation. This would require to study the individual nanomagnets, e.g., with large separation, but the structure of the nanomagnets is the same as supported by TEM analysis

and the height of the cylinders is the same with maximum ±10 nm deviation (checked by SEM before performing the magnetic measurements) for all prepared arrays.

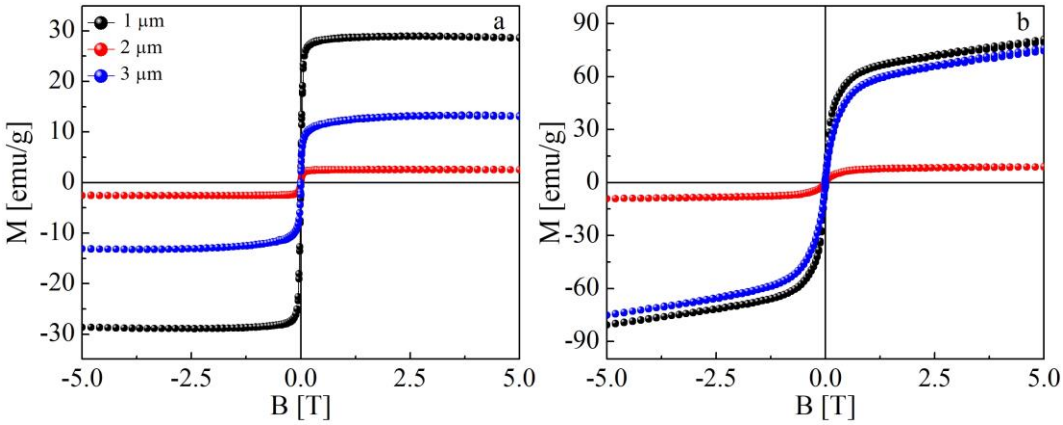

Fig. 8. The dependence of magnetization from the applied external magnetic field for nanomagnet arrays based on Ni_3Pt at a measuring temperature of 300 K: (a) parallel orientation; (b) perpendicular orientation.

As for the magnitude of the coercive force (B_c), its largest value, regardless the geometry of the measurement, is observed for a structure with a period of 3 μm and is 6.82 and 3.73 mT in parallel and perpendicular geometry, respectively. Coercive force for parallel geometry is higher than for perpendicular one and it is in agreement with the general shape of the magnetization curves suggesting that an easy axis of the magnetization is parallel to the substrate.

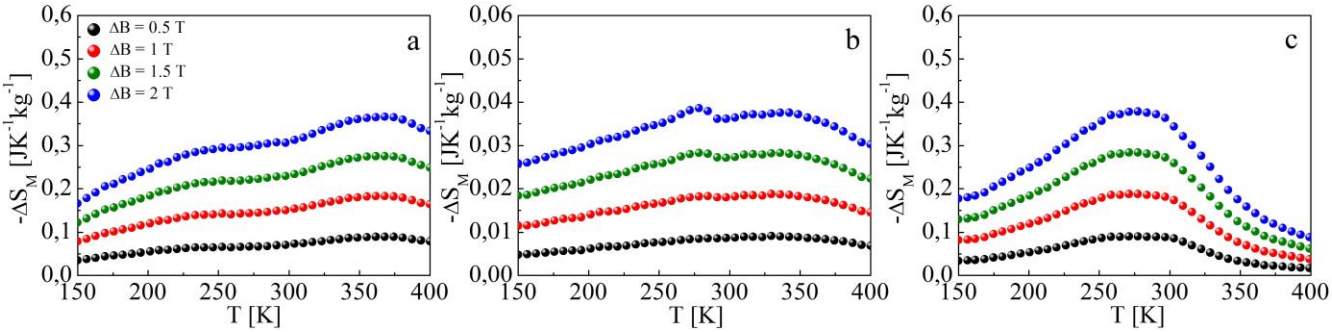

Fig. 9. Temperature dependence of the isothermal entropy change in nanomagnet arrays based on Ni_3Pt at different magnetic fields (parallel orientation) with a different period of structure (a – 1 μm, b – 2 μm, c – 3 μm). The height of the cylinders is 1.2 μm.

Temperature dependences of the entropy change obtained from arrays of nanomagnets with a period of structure 1, 2 and 3 μm and height 1.2 μm for isothermal magnetization from 0 T to different values of the final field spanning from 0.5 T to 2 T, are presented in Figures 9 (a), (b), and (c), respectively. The entropy change was studied for the parallel orientation of the nanomagnet arrays.

The results of the studies showed that the change in the entropy of the system is very sensitive to a change in its period. For example, for magnetic field 2 T, if the period of the array is 1 μm, the maximum value of $-\Delta S_M$ is observed at $T_{max} = 365$ K and is equal to $-\Delta S_M = 0.36$ $JK^{-1}kg^{-1}$, for 2 μm $-\Delta S_M = 0.04$ $JK^{-1}kg^{-1}$ at 275 K, and for 3 μm $-\Delta S_M = 0.38$ $JK^{-1}kg^{-1}$ at 280 K. It should be noted, that for a bulk sample the maximum value of $-\Delta S_M = 0.61$ $JK^{-1}kg^{-1}$ is observed at 370 K. Thus, changing the period of the structure

in arrays of nanomagnets, not only the magnitude of the MCE, but also the operating temperature range may be adjusted. It should be noted that the entropy change is similar for perpendicular orientation, with only small change of $-\Delta S_M$ and with the same T_{max} (data not shown) suggesting a minor influence of magnetic anisotropy on MCE in prepared structures.

The influence of the height of the particles on the magnitude of the change in entropy represented a subsequent step in the presented studies. The temperature dependences of entropy change, obtained from arrays of nanomagnets with the same period of structure, but with a higher height, specifically 1.9 μm, is illustrated in Figure 10. As can be seen, an increase in the height of nanomagnets leads to the appearance of more pronounced entropy change maxima and an increase in the value of $-\Delta S_M$. Thus, for an array of nanomagnets with a period of 1 μm, the maximum value is observed at 365 K and is $-\Delta S_M$ = 0.48 $JK^{-1}kg^{-1}$, for 2 μm $-\Delta S_M$ = 0.16 $JK^{-1}kg^{-1}$ at 250 K, and for 3 μm $-\Delta S_M$ = 0.52 $JK^{-1}kg^{-1}$ at 295 K. The parameters characterizing MCE in prepared arrays of nanomagnets are summarized in Table 1. The observed sensitive and non-monotonic behavior of the arrays indicates pronounced influence of dipolar coupling between nanomagnets on their internal domain structure.

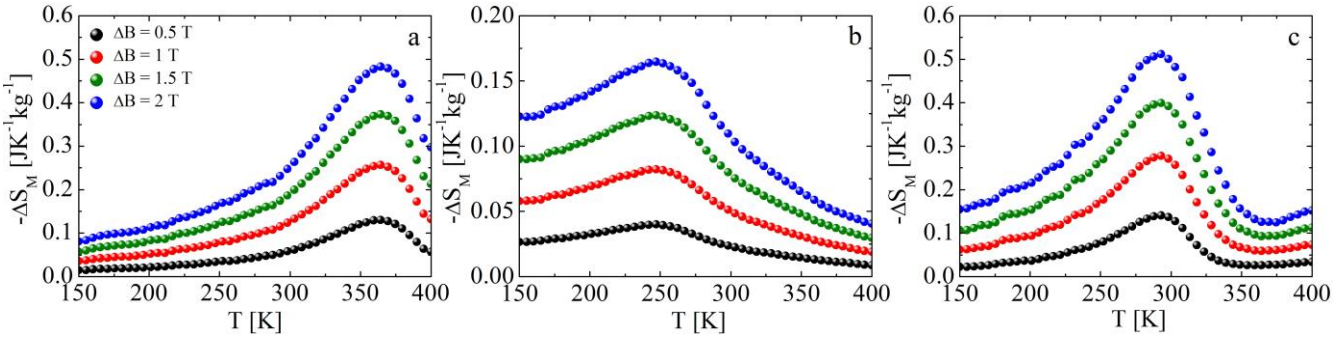

Fig. 10. Temperature dependence of the isothermal entropy change in nanomagnet arrays based on Ni_3Pt at different magnetic fields (parallel orientation) with a different period of structure (a – 1 μm, b – 2 μm, c – 3 μm). The height of the cylinders is 1.9 μm.

Table 1. Dependence of B_c, $-\Delta S_M^{max}$ and T_{max} on geometric parameters of Ni_3Pt nanomagnet arrays

Magnetic parameters	Bulk	The arrays of nanomagnets					
		h =1.2 μm			h =1.9 μm		
		1μm	2 μm	3 μm	1 μm	2 μm	3 μm
B_c, [mT] (parallel, 300 K)	2.291	4.77	6.60	6.82	2.14	3.21	3.11
$-\Delta S_M^{max}$ [$JK^{-1}kg^{-1}$] (ΔB = 2T)	0.61	0.36	0.04	0.38	0.48	0.16	0.52
T_{max} [K]	370	365	275	280	365	250	295

Conclusions

In summary, the technological parameters for fabrication of arrays of Ni_3Pt nanomagnets by electron-beam lithography have been established. Three square arrays of nanomagnets based on Ni_3Pt nanoparticles with a different period of structure (1, 2, 3 μm) and height (1.2 and 1.9 μm) were formed. Studies of the phase composition and crystal structure have shown that the arrays have a phase composition of fcc-Ni_3Pt. Annealing at 800 K in an N_2 atmosphere for 1 hour does not change the phase

composition but leads to the enlargement of the crystallites and to the reduction of defects in the crystal structure. The investigation of the magnetothermal characteristics of nanomagnets has shown a significant effect of the structure period and nanomagnet height on both the magnitude of the magnetocaloric effect and operating temperature range. From the point of optimal temperature range where the maximum of the entropy change appears, the particles with 3 μm period seems to be suitable for room-temperature applications. In the next step, the study of the domain structure of nanomagnets is necessary to reveal the interplay among dipolar coupling and magnetic anisotropies and to be able to enlarge the magnetocaloric response of the arrays.

Acknowledgments

This work has been supported by grant VEGA No. 1/0204/18, the grant of the Slovak Research and Development Agency under the contract No. APVV-14-0073, APVV-17-0059 and by the ERDF EU grant under the contract No. ITMS26220120047. S. Vorobiov acknowledges the financial support provided by the National Scholarship Programme of the Slovak Republic (SAIA).

Reference

1. V. Franco, J.S. Blázquez, J.J. Ipus, J.Y. Law, L.M. Moreno-Ramírez, A. Conde, Magnetocaloric effect: From materials research to refrigeration devices, Prog. Mater. Sci. 93, 112 (2018). DOI: 10.1016/j.pmatsci.2017.10.005
2. O. Tegus, E. Brück, K.H.J. Buschow, F.R. De Boer, Transition-metal-based magnetic refrigerants for room-temperature applications, Nature 415, 150 (2002). DOI: 10.1038/415150a
3. V. Franco, J.S. Bl´azquez, B. Ingale, A. Conde, The magnetocaloric effect and magnetic refrigeration near room temperature: materials and models, Annu. Rev. Mater. Res. 42, 305 (2012). DOI: 10.1146/annurev-matsci-062910-100356
4. M. Balli, S. Jandl, P. Fournier, and A. Kedous-Lebouc, Advanced materials for magnetic cooling: Fundamentals and practical aspects, Appl. Phys. Rev. 4, 021305 (2017). DOI: 10.1063/1.4983612
5. V.V. Khovaylo, V.V. Rodionova, S.N. Shevyrtalov, V. Novosad, Magnetocaloric effect in “reduced” dimensions: Thin films, ribbons, and microwires of Heusler alloys and related compounds, Phys. Status Solidi B 251, 2104 (2014). DOI: 10.1002/pssb.201451217
6. A. Planes, L. Mãosa, M. Acet, Magnetocaloric effect and its relation to shape-memory properties in ferromagnetic Heusler alloys, J. Phys. Condens. Matter. 21, 233201 (2009). DOI: 10.1088/0953-8984/21/23/233201
7. T. Gottschall, K.P. Skokov, D. Benke, M.E. Gruner, O. Gutfleisch, Contradictory role of the magnetic contribution in inverse magnetocaloric Heusler materials, Phys. Rev. B 93, 184431 (2016). DOI: 10.1103/PhysRevB.93.184431
8. T. Krenke, E. Duman, M. Acet, E.F. Wassermann, X. Moya, L. Manosa, A. Planes, Inverse magnetocaloric effect in ferromagnetic Ni-Mn-Sn alloys, Nat. Mater. 4, 450 (2005). DOI: 10.1038/nmat1395
9. D.D. Belyea, M.S. Lucas, E. Michel, J. Horwath, C.W. Miller, Tunable magnetocaloric effect in transition metal alloys, Sci. Rep. 5, 15755 (2015). DOI: 10.1038/srep15755

10. M. Kurniawan, A. Perrin, P. Xu , V. Keylin, M. McHenry, Curie temperature engineering in high entropy alloys for magnetocaloric applications, IEEE Magn. Lett. 7, 7515235 (2016). DOI: 10.1109/LMAG.2016.2592462
11. P. Poddar, J. Gass, D. J. Rebar, S. Srinath, H. Srikanth, S. A. Morrison, and E. E. Carpenter, Magnetocaloric effect in ferrite nanoparticles, J. Magn. Magn. Mater. 307, 227 (2006). DOI: 10.1016/j.jmmm.2006.04.007
12. V. Chaudhary, R.V. Ramanujan, Magnetocaloric properties of Fe-Ni-Cr nanoparticles for active cooling, Sci. Rep. 6, 35156 (2016). DOI: 10.1038/srep35156
13. D. Serantes, D. Baldomir, M. Pereiro, J. Botana, V. M. Prida, B. Hernando, J. E. Arias, J. Rivas, Magnetocaloric effect in magnetic nanoparticle systems: how to choose the best magnetic material?, J. Nanosci. Nanotechnol. 10, 2512, (2010). DOI: 10.1166/jnn.2010.1424
14. D. Baldomir, D. Serantes, M. Pereiro, J. Rivas, C. Vázquez-Vázquez, M. C. Buján-Núñez, J. E. Arias, Role of the magnetic anisotropy in the magnetocaloric effect for a superparamagnetic nanoparticle system: a Monte Carlo study, Phys. Status Solidi A 205, 1343 (2008). DOI: 10.1002/pssa.200778148
15. B. Hernando, J. L. Sanchez-Llamazares, V. M. Prida, D. Baldomir, D. Serantes, M. Ilyn, and J. Gonzalez, Magnetocaloric effect in preferentially textured $Mn_{50}Ni_{40}In_{10}$ melt spun ribbons, Appl. Phys. Lett. 94, 222502 (2009). DOI: 10.1063/1.3147875
16. P.J. Ibarra-Gaytan, C.F. Sánchez-Valdes, J.L. Sánchez Llamazares, P. Álvarez -Alonso, P. Gorria, J.A. Blanco, Texture-induced enhancement of the magnetocaloric response in melt-spun $DyNi_2$ ribbons, Appl. Phys. Lett. 103, 152401 (2013). DOI: 10.1063/1.4824073
17. D. Serantes, V. Vega, W. O. Rosa, V. M. Prida, B. Hernando, M. Pereiro, and D. Baldomir, Interplay between magnetic anisotropy and dipolar interaction in one-dimensional nanomagnets: Optimized magnetocaloric effect, Phys. Rev. B 86, 104431 (2012). DOI: 10.1103/PhysRevB.86.104431
18. M.C. Cadeville, C.E. Dahmani, F. Kern, Magnetism and spatial order in Ni-Pt and Co-Pt alloys, J. Magn. Magn. Mater. 54-57, 1055 (1986). DOI: 10.1016/0304-8853(86)90378-1
19. Y. Liu, C.M. Hangarter, U. Bertocci, T.P. Moffat, Oxygen reduction reaction on electrodeposited $Pt_{100-x}Ni_x$: Influence of alloy composition and dealloying, J. Phys. Chem. C 116, 7848 (2012). DOI: 10.1021/jp300672h
20. X.-G. Lu, B. Sundman, J. Ågren, Thermodynamic assessments of the Ni-Pt and Al-Ni-Pt systems, Calphad 33, 450 (2009). DOI: 10.1016/j.calphad.2009.06.002
21. K.A. Gschneidner Jr., V.K. Pecharsky, A.O. Tsokol, Recent developments in magnetocaloric materials, Rep. Prog. Phys. 68, 1479 (2005). DOI: 10.1088/0034-4885/68/6/R04